Constitutive endocytic cycle of the CB1 cannabinoid receptor.

Christophe Leterrier, Damien Bonnard, Damien Carrel, Jean Rossier, Zsolt Lenkei

THE JOURNAL OF BIOLOGICAL CHEMISTRY
Vol. 279, No. 34, Issue of August 20, pp. 36013–36021, 2004

Printed in U.S.A.

Constitutive Endocytic Cycle of the CB1 Cannabinoid Receptor*[S]

Received for publication, April 9, 2004, and in revised form, June 9, 2004
Published, JBC Papers in Press, June 21, 2004, DOI 10.1074/jbc.M403990200

Christophe Leterrier‡, Damien Bonnard‡, Damien Carrel§, Jean Rossier‡, and Zsolt Lenkei‡¶

From ‡ESPCI-CNRS UMR 7637, Laboratoire Neurobiologie et Diversité Cellulaire, Ecole Supérieure de Physique et de Chimie Industrielles, 10 Rue Vauquelin, 75231 Paris Cedex 05, France and §INSERM U288, NeuroPsychoPharmacologie Moléculaire, Cellulaire et Fonctionnelle, Faculté de Médecine Pitié-Salpêtrière, 91 bd de l'Hôpital, 75634 Paris Cedex 13, France

The CB1 cannabinoid receptor (CB1R) displays a significant level of ligand-independent (*i.e.* constitutive) activity, either when heterologously expressed in non-neuronal cells or in neurons where CB1Rs are endogenous. The present study investigates the consequences of constitutive activity on the intracellular trafficking of CB1R. When transfected in HEK-293 cells, CB1R is present at the plasma membrane, but a substantial proportion (~85%) of receptors is localized in intracellular vesicles. Detailed analysis of CB1-EGFP expressed in HEK-293 cells shows that the intracellular CB1R population is mostly of endocytic origin and that treatment with inverse agonist AM281 traps CB1R at the plasma membrane through a monensin-sensitive recycling pathway. Co-transfection with dominant positive or dominant negative mutants of the small GTPases Rab5 and Rab4, but not Rab11, profoundly modifies the steady-state and ligand-induced intracellular distribution of CB1R, indicating that constitutive endocytosis is Rab5-dependent, whereas constitutive recycling is mediated by Rab4. In conclusion, our results indicate that, due to its natural constitutive activity, CB1R permanently and constitutively cycles between plasma membrane and endosomes, leading to a predominantly intracellular localization at steady state.

G-protein-coupled receptors (GPCRs)[1] represent one of the largest protein superfamilies, with around 1000 receptors in vertebrates (1). The classical paradigm of GPCR function stipulates that GPCRs localize on the cell surface and are activated by the binding of agonist ligands. This leads to G-protein activation and initiates various changes in intracellular signaling pathways. After activation, most GPCRs are endocytosed from cell surface and travel to low pH endosomes, allowing the ligand to detach before the receptor is recycled back to the cell surface or sent through late endosomes to lysosomes for degradation (2). Increasing evidence shows also that some GPCRs are not totally inactive in the absence of ligands but exhibit tonic (*i.e.* constitutive) activity, with elevated basal levels of intracellular signaling (3).

Pharmacological characterization of constitutively active GPCRs leads to the definition of three different ligand classes: agonists, neutral antagonists, and inverse agonists. In the two-state model of receptor activation (4), receptors are in equilibrium between a inactive and an active state. An agonist stabilizes the active state, shifting the receptor population toward activation, a neutral antagonist binds with equal affinity to both active and inactive conformation, whereas an inverse agonist will preferentially stabilize the inactive state. In the absence of ligand, the equilibrium for most GPCRs is shifted strongly to the inactive state, whereas for constitutively active receptors, the equilibrium is shifted toward the active state. Thus, by spontaneously adopting the active conformation, constitutively active GPCRs are able to mobilize cellular signaling pathways in the absence of agonist ligands, and inverse agonist ligands inhibit this basal activation.

The cannabinoid type I receptor (CB1R) is one of the most abundant GPCRs in the central nervous system, with a high level of expression in cortex, hippocampus, basal ganglia, and cerebellum (5). CB1Rs are coupled to $G_{i/o}$-proteins, and activation results in inhibition of cAMP accumulation; mitogen-activated protein kinase activation; inhibition of L, P, Q, and N type Ca^{2+} channels; and activation of Kir type K^+ channels (6). Interestingly, the CB1R, like numerous other GPCRs, displays a high level of constitutive activity (3), either when heterologously expressed in nonneuronal cells (7) or in neurons where CB1Rs are endogenous (8, 9).

In contrast to pharmacology, few studies address the question of intracellular trafficking of constitutively active GPCRs (10, 11). Therefore, we studied the subcellular distribution of the CB1R as well as its trafficking in response to various pharmacological stimulations. We constructed a CB1-EGFP chimera, transiently expressed CB1-EGFP in HEK-293 cells and quantified the subcellular distribution and translocation after different pharmacological treatments. Our results indicate that the constitutively active CB1R undergoes constitutive endocytosis and recycling mediated by the small GTPases Rab5 and Rab4, respectively.

EXPERIMENTAL PROCEDURES

Plasmids, Antibodies, and Reagents—Antibody production was performed by Eurogentec (Herstal, Belgium). The C-Ter antibody was produced by injection of a peptide corresponding to the last 14 C-terminal residues (positions 459–473) of the rat CB1R coupled to keyhole limpet hemocyanin in rabbits followed by affinity purification of sera against the 459–473 peptide. The L14 antibody, kindly provided by Dr. Ken Mackie (University of Washington, Seattle, WA), is directed against the same epitope that is present both in the rat and the mouse receptor. The specificity of the L14 antibody was verified by Western

* The costs of publication of this article were defrayed in part by the payment of page charges. This article must therefore be hereby marked "*advertisement*" in accordance with 18 U.S.C. Section 1734 solely to indicate this fact.

The nucleotide sequence(s) reported in this paper has been submitted to the GenBank™/EBI Data Bank with accession number(s).

[S] The on-line version of this article (available at http://www.jbc.org) contains one movie.

¶ To whom correspondence should be addressed. Tel.: 33-1-40-79-51-84; Fax: 33-1-40-79-47-57; E-mail: zsolt.lenkei@espci.fr.

[1] The abbreviations used are: GPCR, G protein-coupled receptor; CB1R, CB1 cannabinoid receptor; GFP, green fluorescent protein; EGFP, enhanced GFP; MFR, membrane fluorescence ratio; Tf, transferrin; TfR, Tf receptor; WIN, WIN55,212-2; MβCD, methyl-β-cyclodextrin; ER, endoplasmic reticulum.

blotting and immunohistochemistry on CB1+/+ and CB1−/− mice.[2] The N-Ter antibody was produced by Double-X program (Eurogentec) with coinjection of keyhole limpet hemocyanin peptides corresponding to residues 22–36 and 53–67 of the receptor in rabbits, followed by affinity purification of the sera against the 53–67 peptide. The anti-human transferrin receptor OKT9 antibody was from ATCC, and the Cy3-conjugated transferrin was a gift from Dr. Alice Dautry (Institut Pasteur, Paris, France). Anti-Golgi matrix 130 protein (GM130; Golgi marker) was from Transduction Laboratories, the anti-protein-disulfide isomerase (endoplasmic reticulum (ER) marker) was from Stressgene, and the 6C4 antibody (marker of late endosomes (12)) was a gift of Dr. Bruno Goud (Institut Curie, Paris, France). The Rab-EGFP (13) plasmids were generously provided by Dr. Robert Lodge (Université du Quebec, Laval). Alexa®-labeled secondary antibodies were from Molecular Probes, Inc. (Eugene, OR). Cannabinoid ligands were from Tocris. All other chemicals were from Sigma.

DNA Constructs—The CB1R sequence was amplified without its stop codon from rat genomic DNA using the primers 5′-TTTGGATCCATGAAGTCGATCATCCTAGAT and 3′-TTTACCGGTAGAGCCTCGGCGGACGT and inserted between the AgeI and BamHI sites of the pEGFP-N1 plasmid (Clontech), generating the CB1-EFGP construct. The CB1-WT construct coding for the untagged CB1R was obtained by inserting a stop codon into the CB1-EGFP sequence at the end of the CB1R coding sequence using the QuikChange™ mutagenesis system (Stratagene). All constructs were verified by full-length sequencing.

Cell Culture and Transfection—HEK-293 cells (ATCC CRL-1573) cultivated in minimal essential medium, 7.5% fetal calf serum (Invitrogen) were transfected in 6-well plates with 0.8 μg of CB1-EGFP plasmid DNA using Effectene reagent (Qiagen). For the Rab-EGFP experiments, cells were co-transfected with 0.4 μg of Rab-EGFP plasmid. Lilly pork kidney cells (LLC-PK1; ATCC CL-101) were grown and transfected as previously described (14). Neuroblastoma SHSY-5Y cells (ATCC CRL-2266) were grown in Dulbecco's modified Eagle's medium supplemented with 10% fetal calf serum and transfected with 0.8 μg of plasmid CB1-EGFP DNA using Effectene.

Pharmacological Assays in HEK-293 Cells—For the cAMP assay, a bioluminescent assay was performed following the manufacturer's instructions (Tropix). Briefly, cells seeded in precoated 96-well plates were preincubated the next day 15 min at 37 °C with phosphate-buffered saline, 0.1% bovine serum albumin, 1 mM isobutylmethylxanthine, 1 μM RO20-1724 and then incubated for 15 min at 37 °C in the presence of 10 μM forskolin and processed for bioluminescent assay. For CB1R trafficking experiments, cells were seeded 48–72 h after transfection on polyallylamine-treated chambered coverglass 8-well slides (Labtek, Nunc) and assayed as described previously (11). Briefly, after a 1-h preincubation with 70 μM cycloheximide, cells were incubated for 15 min at 4 °C in Earle's buffer (140 mM NaCl, 5 mM KCl, 1.8 mM $CaCl_2$, 0.9 mM $MgCl_2{\cdot}6H_2O$, 25 mM HEPES, pH 7.6) supplemented with 0.2% bovine serum albumin, 0.01% glucose, 0.08 mM phenanthroline, and 70 μM cycloheximide. Cells were then incubated with ligands in supplemented Earle's buffer for 30 min at 4 °C, before being incubated at 37 °C for various periods of time. After incubation, cells were washed with ice-cold Earle's buffer and fixed.

Immunohistochemistry—The specificity of the C-Ter, L14, and N-Ter antibodies was verified by colocalization of immunostaining with GFP fluorescence in CB1-EGFP-expressing cells, and negative controls were performed either by omitting the primary antibody or by depleting the primary antibody with corresponding blocking peptides, resulting in a complete loss of immunolabeling. The staining pattern of the C-Ter antibody and that of the L14 antibody were similar. For immunostaining of fixed cells, HEK-293 cells were fixed for 15 min in phosphate-buffered saline, 4% paraformaldehyde, permeabilized with 0.1% Triton X-100, immunostained for 1 h for CB1R using the C-Ter or L14 primary antibody diluted to 1:1000 at room temperature, and incubated for 30 min with anti-rabbit Alexa® 568 secondary antibody diluted to 1:400 at room temperature. For live immunostaining of surface receptors, cells were incubated for 5 min at the end of treatments in supplemented minimal essential medium with N-Ter antibody diluted to 1:400. Cells were fixed with phosphate-buffered saline, 4% paraformaldehyde and incubated for 30 min at room temperature with anti-rabbit Alexa® 568 secondary antibody diluted to 1:400. For live antibody feeding, cells were incubated for 2 h at 37 °C in supplemented minimal essential medium with N-Ter antibody diluted to 1:200 and fixed with 4% paraformaldehyde. Cells were then incubated with anti-rabbit Alexa® 568 secondary antibody without or after permeabilization with 0.1% Triton X-100. For transferrin uptake experiments, cells were placed in serum-free minimal essential medium for 1 h and incubated with Cy3-Tf diluted to 1:400 for 1 h at 37 °C before fixation.

Cell Microscopy—For confocal microscopy, images (1024 × 1024 pixels) of individual cells were obtained on a Leica TCS NT confocal laser-scanning microscope by the use of a × 63, numerical aperture 1.4 oil immersion objective and × 4 zoom, resulting in a pixel size of 38.75 nm. Excitation was done at 488 nm, and fluorescence detection used a 525 ± 25-nm bandpass filter. Each image was realized on the equatorial cross-section through the cell that maximized nuclear diameter. Cells were randomly chosen in the well for each condition, with phenotypic consideration to avoid dead, dividing, or highly CB1R-overexpressing cells. In our protocol, cells are fixed 2–4 h (depending from the incubation length) after seeding, displaying a rather spherical form that allows precise equatorial optical sectioning and facilitates quantification. Co-detection of EGFP and red fluorescence (Cy3 or Alexa® 568) was done by excitation at 488 and 568 nm, using simultaneous detection with 525 ± 25-nm bandpass and >590-nm longpass filters.

For live cell imaging, CB1-EGFP-transfected HEK-293 cells were imaged on the ultrafast 4/5D deconvolution imaging system at Institut Curie (Paris, France) (15), using a Leica DM-IRBE microscope equipped with a × 100, numerical aperture 1.4 objective and a temperature-controlled box at 37 °C (The Box & The Cube, LIS). Stacks of images with a 0.2-μm Z step (~10–15 frames/stack) were acquired every 3 s for 5 min. After deconvolution (15), stacks were projected along the z axis using Metamorph Software (Universal Imaging Corp.).

Image Quantification—Confocal images were used to quantify the subcellular distribution and translocation of CB1R (11, 16). In-house-developed macro algorithms (available on request), written for the public domain Object Image software (available on the World Wide Web at simon.bio.uva.nl/object-image.html), were used to measure the subcellular distribution of the CB1Rs in HEK-293 cells. We measured mean fluorescence density values S, C, and N, corresponding to the surface (measured from the edge of the cell to 300 nm inside), cytoplasm, and nucleus of the cell. The nuclear fluorescence N, corresponding to the background, was subtracted from the S and C values, which, once multiplied by the respective areas, yielded the S' and C' total specific fluorescence. The displayed result is the S'/C' ratio that we call the membrane fluorescence ratio (MFR). The mean cell fluorescence, measuring the CB1R expression level in individual cells, was obtained by measuring the background-corrected mean density of the total cellular area (surface and cytoplasm).

RESULTS

CB1-EGFP Is Functional and Displays a Predominantly Intracellular Localization in HEK-293 Cells—In order to directly visualize and quantify the traffic of the CB1R, we created a chimeric protein by fusing EGFP to the C terminus end of the CB1R (CB1-EGFP). CB1R activation results in cAMP inhibition by negatively regulating adenylate cyclase activity (6). In nontransfected HEK-293 cells, forskolin stimulation induces a 37 ± 1.03-fold accumulation of cAMP. In contrast, cells transiently expressing the wild type CB1R (CB1-WT) or CB1-EGFP show a 2-fold lower level of cAMP accumulation, with a stimulation factor of 17.3 ± 0.51 and 19.8 ± 0.28, respectively (Fig. 1*A*). Thus, CB1R exerts a constitutive inhibitory effect on cAMP accumulation in HEK-293 cells, consistent with previous data obtained in CHO cells (7) or rat brain membrane preparations (17). This effect is similar for CB1-WT and CB1-EGFP, showing that CB1-EGFP is functional.

Strikingly, observation of CB1-EGFP-expressing HEK-293 cells by confocal microscopy shows that CB1-EGFP receptors are localized both on the plasma membrane and in intracellular vesicles (Fig. 1*B*). We quantified CB1-EGFP subcellular distribution on confocal images by measuring the MFR, which is the ratio of plasma membrane fluorescence over intracellular fluorescence (see "Experimental Procedures"). Quantification of CB1-EGFP distribution on equatorial confocal sections of individual cells leads to a MFR of 0.19 ± 0.02 for control cells in a typical experiment (see Figs. 1*E* and 4, *A* (*a*) and *B*). If we translate this value to express the percentage of CB1Rs that are intracellular, the result shows that ~85% of CB1Rs are

[2] K. Mackie, personal communication.

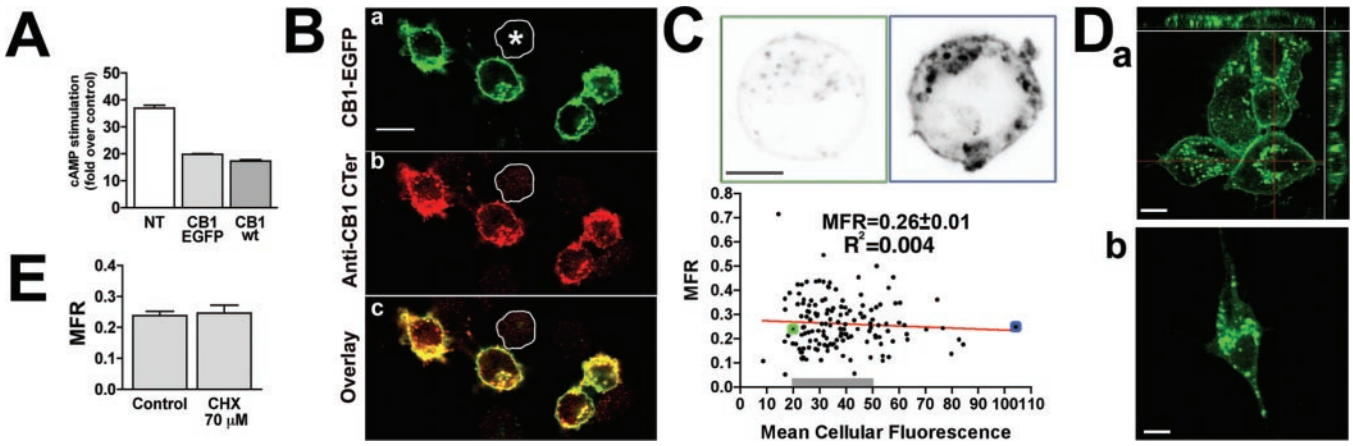

FIG. 1. **CB1-EGFP is functional and localizes in several cell lines to both the plasma membrane and endosomes.** *A*, forskolin-stimulated cAMP production of HEK-293 cells, untransfected (*NT*) or transfected with CB1-EGFP or CB1-WT. *B*, HEK-293 transiently expressing CB1-EGFP (*a*), stained with C-Ter antibody (*b*), with overlay (*c*). *Scale bar*, 20 μm. Note that untransfected cells (*) are not labeled by the C-Ter antibody, showing its specificity (*b*). *C*, graph showing the MFR (ratio of the corrected total fluorescences of surface *versus* cytoplasm, as described under "Experimental Procedures") versus the mean cellular intensity (as a measure of CB1-EGFP expression level in each cell) for 145 CB1-EGFP-transfected HEK-293 cells. The MFR and the expression level are not correlated ($R^2 < 0.005$). The *gray bar* shows the range of qualifying transfection levels for quantification in subsequent experiments (mean cellular fluorescence from ~20 to ~50). On *top* are shown two cells that correspond to a very low CB1R-expressing cell (*left*, *green dot* on *graph*) and a highly CB1R-expressing cell (*right*, *blue dot* on *graph*). The two images were acquired and post-treated identically, and the two cells show the same distribution pattern for CB1R. *Scale bar*, 5 μm. *D*, *a*, confocal image of epithelial LLC-PK1 cells expressing CB1-EGFP. *Scale bar*, 10 μm. *b*, confocal image of a neuroblastoma SHSY-5Y cell expressing CB1-EGFP. *Scale bar*, 10 μm. *E*, quantification of the MFR for CB1-EGFP-expressing cells after a 4-h incubation with or without 70 μM cycloheximide (*CHX*). $n = 8$ cells. Results are expressed as mean ± S.E. and are representative of two independent experiments.

localized to cytoplasmic vesicles in the equatorial plane of control cells.

This distribution could result from heterologous overexpression of CB1R in HEK-293 cells. HEK-293 cells transiently transfected with CB1-EGFP show a large range of expression levels. We thus quantified 145 cells showing large variations in the mean cell fluorescence (indicating expression level) and of membrane fluorescence ratio (representing subcellular distribution). The resulting graph (Fig. 1*C*) shows that there is no correlation between the expression level and the membrane/cytoplasm distribution, since the correlation coefficient R^2 is very low (<0.005) and the slope of the correlation is weakly negative, not significantly different from zero, showing that the MFR does not vary with the mean cell fluorescence. Moreover, GFP-tagged AT_{1A} angiotensin II (11) or somatostatin SSTR2 receptors expressed at the same levels in HEK-293 cells localize predominantly at the plasma membrane (data not shown), showing that overexpression is not the cause of intracellular receptor accumulation. Furthermore, it is not due to the GFP tag, since untagged CB1-WT receptors detected by immunohistochemistry display the same intracellular distribution (data not shown). Finally, a similar distribution is observed in cell lines other than HEK-293 such as polarized epithelial LLC-PK1 cells (14) (Fig. 1*D*, *a*) or SHSY-5Y neuroblastoma cells (Fig. 1*D*, *b*), where CB1-EGFP also localizes predominantly in intracellular vesicles.

Intracellular CB1R Distribution Indicates Endocytic Origin—Intracellular CB1R localization has been previously reported (18, 19), and these intracellular receptors could presumably correspond to maturing receptors in the neosynthetic pathway. To assess the proportion of newly synthesized intracellular CB1R receptors, we monitored the distribution of CB1-EGFP receptors after continuous treatment (1–4 h) with cycloheximide, an inhibitor of protein synthesis. This treatment does not change the distribution of CB1Rs (Fig. 1*E*), suggesting that neosynthesis is not the primary source of intracellular CB1R fluorescence.

We also performed labeling of various intracellular compartments of cycloheximide-treated CB1-EGFP-expressing cells (Fig. 2): Golgi apparatus with anti-GM130 antibody (*a–d*), ER with anti-protein-disulfide isomerase antibody (*e–h*), transferrin receptor (TfR)-containing endosomes with anti-TfR OKT9 antibody (*i–l*), endocytosed transferrin (Tf) with Cy3-

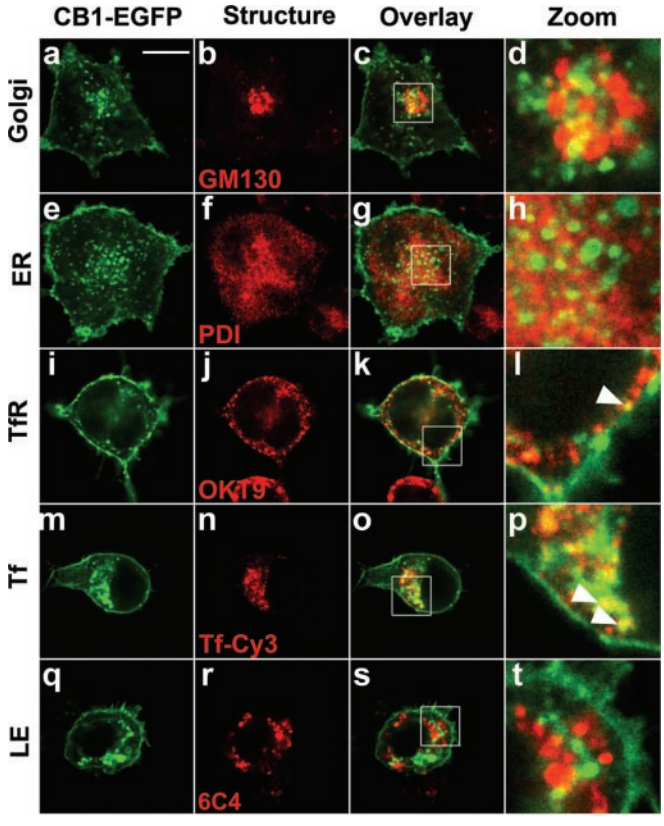

FIG. 2. **Immunolabeling pattern of intracellular CB1R suggest endocytic origin.** CB1-EGFP-expressing cells with immunostaining of intracellular structures: Golgi apparatus (*a–d*), ER (*e–h*), TfR (*i–l*), endocytosed Cy3-transferrin-containing endosomes (*Tf*; *m–p*), and late endosomes (*LE*; *q–t*). *Scale bar*, 10 μm. *Insets* (*d*, *h*, *l*, *p*, and *t*) show higher magnification of the zone *boxed* in *c*, *g*, *k*, *o*, and *s*, with colocalization of receptor clusters with TfR- or Tf-positive endosomes (*arrowheads*).

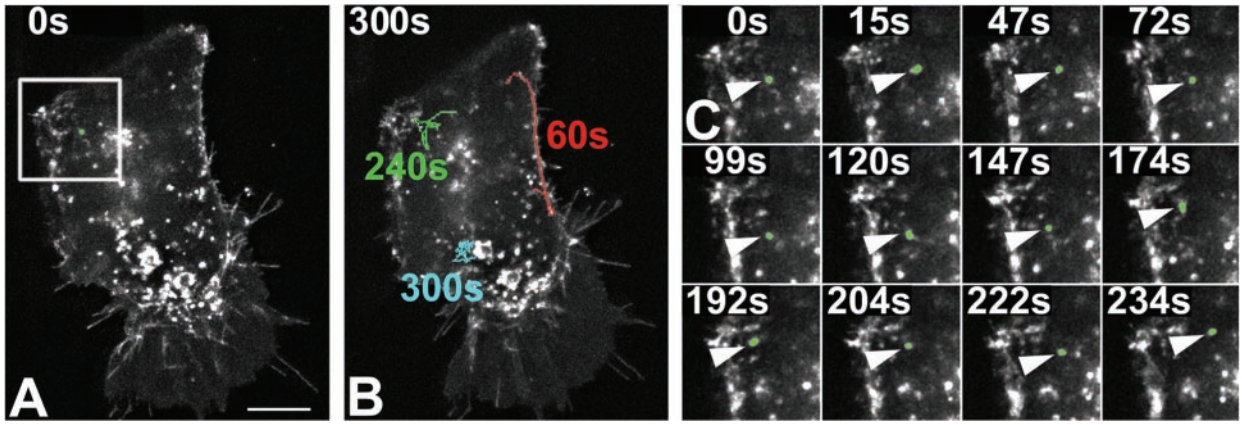

FIG. 3. **Live imaging of CB1-EGFP in HEK-293 cells.** Four-dimensional deconvoluted time lapse imaging of a HEK-293 cell expressing CB1-EGFP. Z-stacks of 15 images, with a 0.2-μm step, were acquired every 3 s for 5 min. Shown are maximum projections of deconvoluted stacks. *A*, cell at 0 s. *Scale bar*, 10 μm. *B*, cell at the end of acquisition (300 s), with trajectories of three vesicles during acquisition. The times on trajectories correspond to the total times during which the vesicle could be tracked. *C*, zoom corresponding to *box* on whole cell image (*A*) at different time points, showing a mobile endosome highlighted in *green* (*arrowhead*, *green trajectory* on *B*).

conjugated Tf (*m–p*), and late endosomes with 6C4 antibody (*q–t*). CB1Rs do not show major colocalization with neosynthesis (Golgi and ER) or with degradative (late endosomes) pathways. Intracellular CB1R-positive vesicles are morphologically similar to TfR-positive endosomes, and several TfR- or Tf-positive endosomes contain CB1R (Fig. 2, *i–p*, *arrowheads* in *l* and *p*), but CB1Rs do not significantly colocalize with TfRs that appear in perinuclear recycling endosomes. Thus, the majority of intracellular CB1Rs are not likely to correspond to maturing or degrading receptors but rather have an endocytic origin.

Dynamics of CB1-EGFP in Living HEK-293 Cells—Live cell imaging using four-dimensional deconvolution microscopy allowed us to gain insights into dynamics of CB1-EGFP in HEK cells (Fig. 3 and Movie 1 in the Supplementary Material). Using fast acquisition rates (one Z-stack every 3 s), we observed living CB1-EGFP-transfected HEK-293 cells. This allowed us to track CB1-EGFP-containing vesicles moving across the cytoplasm with remarkable spatial and temporal resolution (Fig. 3, *B* and *C*). Vesicles show various dynamics: certain ones are rapidly moving over long distances across cytoplasm (*red trajectory* in Fig. 3*B*), and others show rapid movements between periods of relative immobility (see *green trajectory* in Fig. 3*B* and montage in Fig. 3*C*), whereas others are more static (see *blue trajectory* in Fig. 3*B*). Events of fission and fusion between vesicles or with plasma membrane can also be observed. Thus, CB1-EGFP show very fast dynamics in HEK-293 cells that are compatible with possible constitutive trafficking of CB1R between plasma membrane and cytoplasm.

CB1Rs Redistribute upon Treatment with Agonist and Inverse Agonist—Using confocal microscopy, we monitored the effects of various cannabinoid ligands on the subcellular distribution of CB1-EGFP by measuring the MFR variation. In parallel, we labeled surface receptors with the N-Ter antibody, directed against an extracellular epitope in the amino terminus of the receptor. Incubation for 3 h with agonist WIN55,212-2 (WIN; 330 nM) (Fig. 4*A*) or CP 55,940 (1 μM, data not shown) leads to complete endocytosis of the plasma membrane-localized population of CB1Rs (Fig. 4, *A* and *B*), with a 75% decrease of the MFR and an almost complete disappearance of surface receptor labeling (Fig. 4*A*, *e*). Two other CB1R agonists: methanandamide (*mAn*), a stable analog of the endocannabinoid anandamide, and the putative endocannabinoid noladin ether (*NE*) also provoke CB1R endocytosis, with a decrease of the MFR to values close to that induced by WIN (Fig. 4*B*). These results are consistent with previous observations of CB1R endocytosis (18, 20–22).

Next, we investigated the effects of the cannabinoid inverse agonist AM281 (23), an analog of SR141716A (Rimonabant). AM281 is able to antagonize endocytosis induced by the agonist WIN (Fig. 4*B*), restoring the MFR of control cells. Importantly, when applied alone, AM281 (7 μM for 3 h) induces translocation of intracellular CB1Rs toward the plasma membrane, clearing the cytoplasm of CB1R-containing vesicles (Fig. 4*A*, *g*). The antibody-labeled surface population rises (Fig. 4*A*, *h*), accompanied by a 2-fold increase of the MFR (Fig. 4*B*). Since the amount of total CB1-EGFP fluorescence does not change notably after incubation with AM281 (data not shown), the up-regulated plasma membrane-localized CB1Rs are most likely to be translocated (externalized) from intracellular endosomes. The structurally related inverse agonist AM251 has a similar effect (data not shown). Control experiments using immunodetection of the untagged CB1-WT receptor demonstrated that untagged CB1R trafficking induced by WIN and AM281 (data not shown) is identical to CB1-EGFP.

To further characterize CB1R endocytosis and externalization, concentration-response and kinetic curves for translocation induced by WIN and AM281 were established (Fig. 4*C*). WIN-induced endocytosis is dose-dependent with an EC_{50} of 2.07 $\pm$ 0.01 nM, and AM281 induces dose-dependent externalization with an EC_{50} of 3.41 $\pm$ 0.22 nM (Fig. 4*C*, *a*), values that are close to the K_d reported for WIN and AM281 (24, 25). Interestingly, kinetics of CB1R endocytosis and externalization (Fig. 4*C*, *b*) are clearly different. WIN induces an exponential decay of the membrane population of CB1Rs, with a half-time of 4.3 $\pm$ 0.6 min, leading to total endocytosis after 30 min, a value that is typical for GPCR endocytosis (26). AM281-induced externalization is slower, with a linear increase of the MFR ratio reaching a plateau after 2 h.

CB1R Is Constitutively Endocytosed and AM281-induced Externalization Is Recycling-dependent—In order to directly demonstrate constitutive endocytosis, we incubated live CB1R-expressing HEK-293 cells with the N-Ter antibody. After 2 h of incubation at 37 °C, the antibody is detected in intracellular vesicles (Fig. 5*A*, *e*), showing constitutive endocytosis of CB1R. One could predict that if receptors were constitutively endocytosed, blocking endocytosis without interfering with recycling would lead to accumulation of receptors on the plasma membrane, mimicking the effect of AM281. Acute depletion of plasma membrane cholesterol content by the use of methyl-β-cyclodextrin (MβCD) has been shown to inhibit clathrin-mediated endocytosis of the TfR, whereas recycling of the TfR is not modified by this treatment (27). Indeed, after incubation with

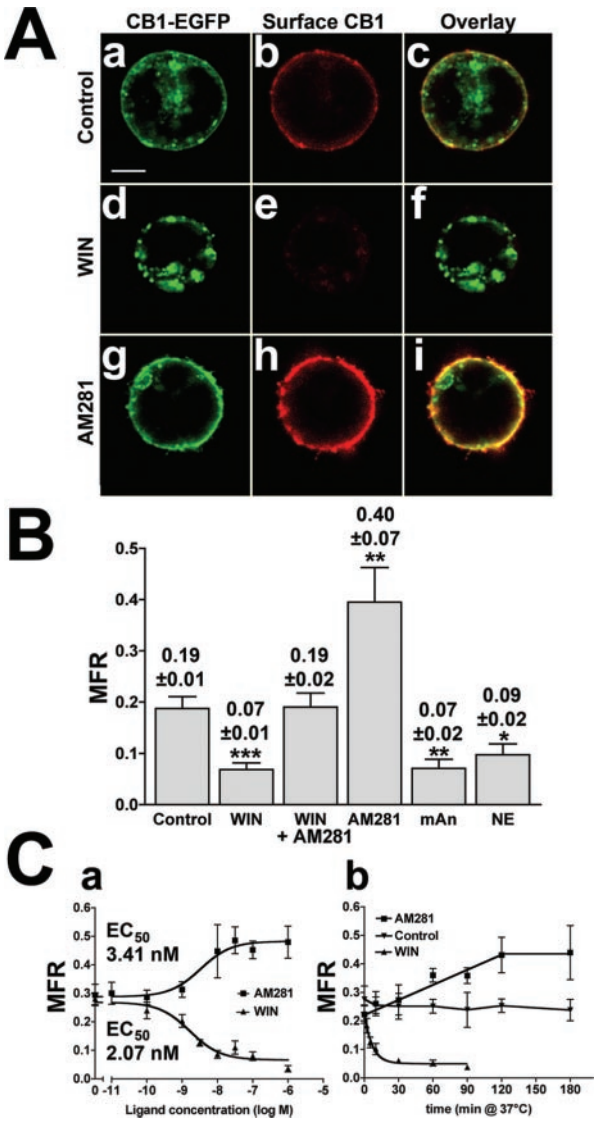

FIG. 4. **Translocation of CB1R after pharmacological treatments in HEK-293 cells.** *A*, confocal images of HEK-293 cells transfected with CB1-EGFP and treated for 3 h at 37 °C in the presence of cycloheximide. *Scale bar*, 5 μm. *a–c*, equatorial section of an untreated cell showing EGFP fluorescence on the plasma membrane and in small vesicules. *a*, CB1-EGFP fluorescence; *b*, surface receptors detected with N-Ter antibody; *c*, overlay. *d–f*, endocytosis after incubation with 330 nM agonist WIN. *g–i*, externalization after treatment with 7 μM inverse agonist AM281. *B*, quantification of the subcellular distribution of CB1-EGFP following incubation with ligands at a concentration corresponding to 100 times K_d: 330 nM for WIN, 9 μM for methanandamide (*mAn*), and 2 μM for noladin ether (*NE*). Inverse agonist AM281 was applied at a 500 K_d concentration (7 μM). For each condition, the MFR was measured for a population of 8–12 cells. *C*, *a*, concentration-response curves for WIN and AM281 effects on subcellular CB1-EGFP distribution. Cells were preincubated for 30 min at 4 °C with various concentration of ligand and then incubated at 37 °C for 20 min without ligand for WIN (pulse-chase) or 3 h in the presence of ligand for AM281. *b*, time course of the effects of WIN and AM281 on subcellular CB1R distribution. Cells were preincubated for 30 min at 4 °C with 330 nM WIN or 7 μM AM281 and then incubated at 37 °C for various periods of time in the absence (WIN) or presence (AM281) of ligand. Results are expressed as mean ± S.E. and are representative of two independent experiments. *, $p < 0.05$; **, $p < 0.01$; ***, $p < 0.001$, compared with control.

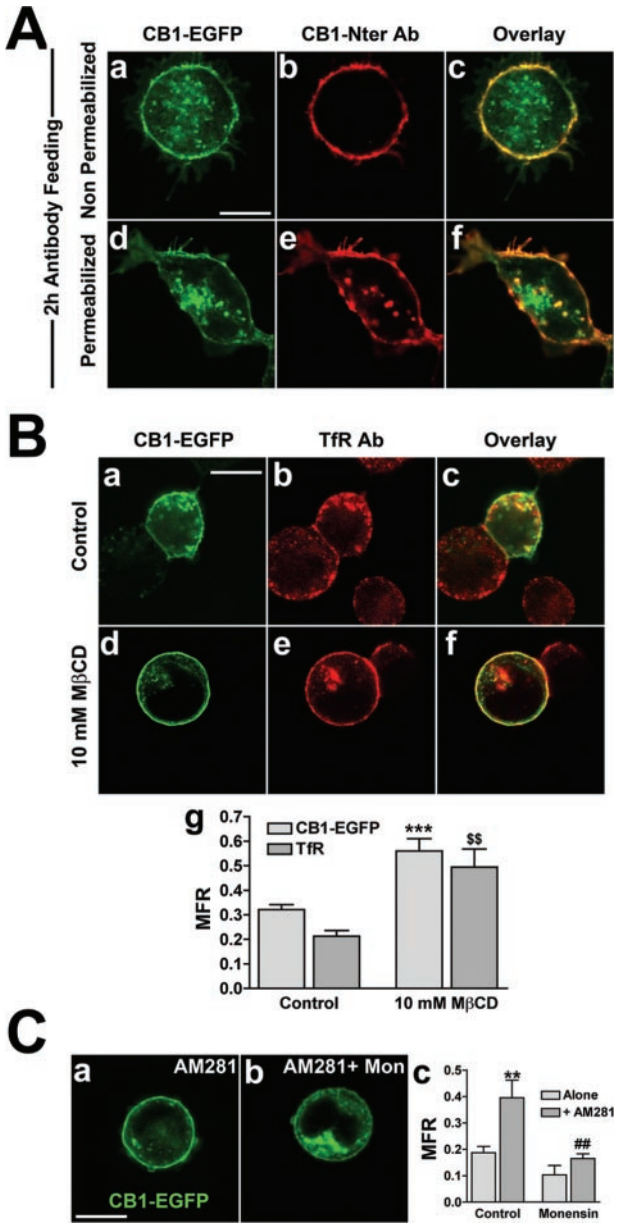

FIG. 5. **CB1R is constitutively endocytosed in HEK-293 cells, and AM281-induced externalization is recycling-dependent.** *A*, live N-Ter antibody feeding of CB1-EGFP expressing cells. Cells were incubated for 2 h with N-ter antibody and fixed. Immunolabeling was performed without (*a–c*) or after (*d–f*) permeabilization with Triton X-100. *Scale bar*, 10 μm. *B*, effect of inhibition of endocytosis by acute depletion of plasma membrane cholesterol on the subcellular distribution of TfR and CB1R. Confocal images of CB1-EGFP-transfected HEK-293 cells fixed after 2 h of incubation at 37 °C with vehicle (*a–c*), 10 mM MβCD for acute depletion of plasma membrane cholesterol (*d–f*), CB1-EGFP fluorescence (*a* and *d*), TfR immunolabeling (*b* and *e*), and overlay (*c* and *f*). *Scale bar*, 10 μm. *g*, quantification of the effect of MβCD treatment (n = 8–15 cells). Results are expressed as mean ± S.E. and are representative of two independent experiments. ***, $p < 0.001$ for significance of difference between control and MβCD treatment for CB1-EGFP. $$, $p < 0.01$ for significance between control and MβCD treatment for TfR labeling. *C*, effects of recycling inhibitor monensin on CB1R externalization. Confocal images of CB1-EGFP transfected HEK-293 cells and treated 3 h at 37 °C with 7 μM inverse agonist AM281 alone (*a*) or together with monensin (*Mon*; 70 nM) (*b*). *Scale bar*, 10 μm. *c*, quantification of the effects of monensin on the subcellular distribution and AM281-induced externalization of CB1-EGFP (n = 8 cells). Results are expressed as mean ± S.E. and are representative of two independent experiments. **, $p < 0.01$; for significance of difference between distribution with vehicle-treated cells. ##, $p < 0.01$ for significance between inverse agonist-induced externalization with and without recycling inhibitor. *Scale bar*, 5 μm.

10 mM MβCD for 2 h, TfR endocytosis is strongly inhibited, and recycled TfRs accumulate on the plasma membrane (Fig. 5*B*, *e* and *g*). In a similar way, CB1Rs are strongly externalized by this treatment (Fig. 5*B*, *d* and *g*), further indicating that the formation of the intracellular pool of receptors is a result of constitutive endocytosis.

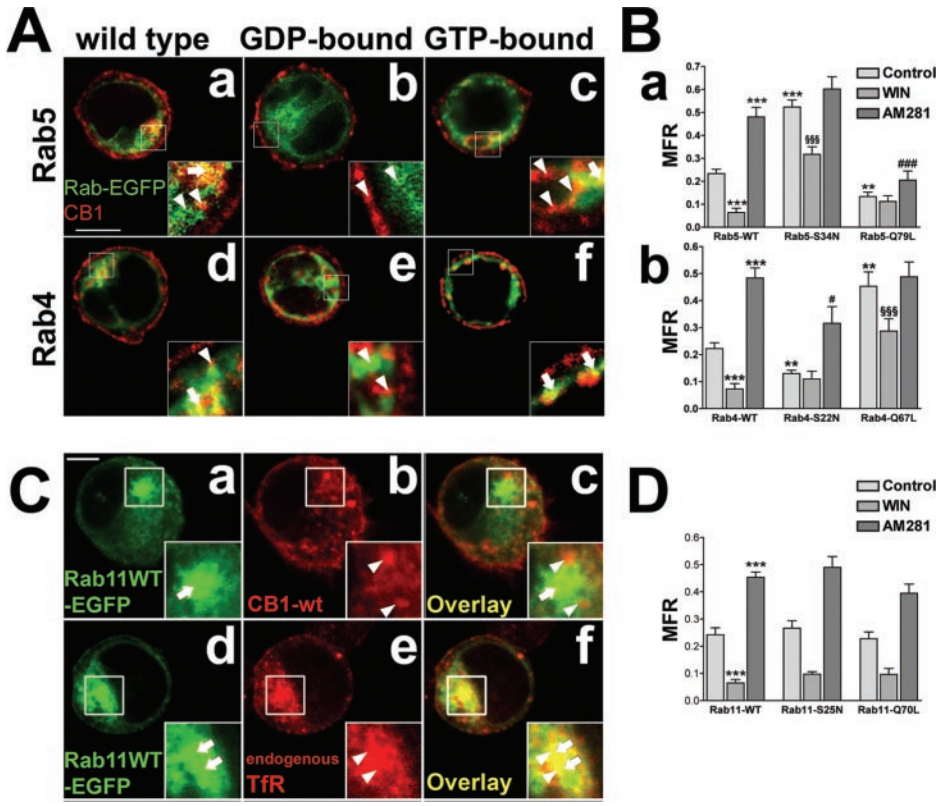

FIG. 6. **The constitutive endocytosis/recycling cycle of CB1R is regulated by Rab5 and Rab4 GTPases.** HEK-293 cells were cotransfected with the CB1-WT receptor and EGFP-tagged wild type (*RabWT*) or mutant Rab GTPases. Two days later, cells were incubated for 3 h in the presence of vehicle, 660 nM WIN, or 7 μM AM281, permeabilized, and immunostained for CB1R using the L14 antibody and Alexa®-568 anti-rabbit secondary antibody. *A*, confocal images of representative cells for control conditions with different mutants (*columns*) of Rab5 or Rab4 GTPases (*rows*). *Green*, Rab-EGFP; *red*, CB1R immunolabeling; *scale bar*, 5 μm. The *insets* show higher magnification of cells, with colocalization of receptor clusters with Rab-positive endosomes (*arrows*) or noncolocalized structures (*arrowheads*). *B*, quantification of the receptor distribution in cells expressing Rab5 (*a*) or Rab4 (*b*) mutants after a 3-h incubation at 37 °C with vehicle (*Control*), 660 nM WIN, or 7 μM AM281 (n = 8 cells). Results are expressed as mean ± S.E. and are representative of two independent experiments. **, $p < 0.01$; ***, $p < 0.001$, compared with vehicle-treated, RabWT-transfected cells; $$$, $p < 0.001$ compared with WIN-treated, RabWT-transfected cells; #, $p < 0.05$; ###, $p < 0.001$ compared with AM281-treated, RabWT-transfected cells. *C*, HEK-293 cells expressing Rab11WT-EGFP and CB1-WT immunolabeled for CB1R with the L14 antibody (*a–c*) or expressing Rab11WT-EGFP alone immunolabeled for endogenous TfR using the OKT9 antibody (*d–f*). *Scale bar*, 5 μm. The *insets* show higher magnification of cells; Rab11 is present mostly in perinuclear recycling endosomes (*a* and *d*, *arrows*), and CB1Rs do not significantly colocalize (*b*, *arrowheads*), whereas TfRs show consistent colocalization (*e*, *arrowheads*) with this compartment. *D*, quantification of the receptor distribution in cells expressing Rab11 mutants after a 3-h incubation at 37 °C with vehicle (*Control*), 660 nM WIN, or 7 μM AM281 (n = 8 cells). Results are expressed as mean ± S.E. and are representative of two independent experiments. ***, $p < 0.001$ compared with vehicle-treated, RabWT-transfected cells.

If AM281 acts by sequestering CB1Rs that have been delivered to the plasma membrane by constitutive recycling, blocking the recycling process would antagonize the AM281 effect. Monensin, a potent inhibitor of recycling (11, 25), strongly inhibits the AM281-induced externalization (Fig. 5*C*). In addition, other compounds that have been shown to inhibit recycling of the TfR receptor (28, 29) and of the AT_{1A} angiotensin II receptor (13), the phosphoinositide 3-kinase inhibitors wortmannin and LY294002, and brefeldin A also inhibit CB1R externalization induced by AM281 (data not shown). These compounds have a broad range of cellular effects; they unravel the constitutive endocytosis of CB1R and indicate that AM281 may act through constitutive recycling but do not allow unambiguous identification of the intracellular pathways involved.

Constitutive Cycling of CB1R Is Regulated by the Small GTPases Rab5 and Rab4 but Not Rab11—We thus sought to identify the molecular partners that control CB1R endocytosis and recycling by studying the role of three members of the Rab family of small GTPases (30). Rab5 is required for the delivery of membrane proteins from the plasma membrane to early endosomes (31), Rab11 has been shown to control the slow component of recycling from the perinuclear recycling endosomes to the plasma membrane (32), whereas Rab4 was suggested to play a role in both slow and fast recycling to the plasma membrane (33). Rab4, Rab5, and Rab11 have been shown to control the agonist-mediated endocytosis and recycling of many GPCRs (34, 35). However, the role of these Rabs has never been studied to specifically address constitutive trafficking of a constitutively active GPCR. In HEK-293 cells expressing EGFP-tagged Rab5, Rab4, or Rab11, we observed that cotransfected CB1Rs colocalized mainly with Rab5 and Rab4 (Fig. 6*A*, *arrows*) but not significantly with Rab11 (Fig. 6*C*). Control experiments show that the amount of wild type Rab-EGFP plasmids used for cotransfection does not interfere with steady-state CB1R localization and ligand-induced translocation (Fig. 6, *B* and *D*; MFR for Rab4-WT-, Rab5-WT-, and Rab11-WT-transfected cells is not significantly different from the controls shown in Fig. 4*B*).

We then used GDP-bound (dominant negative) and GTP-bound (dominant active) Rab mutants fused with EGFP (13) to assess the influence of each Rab protein on the distribution of CB1Rs and their ligand-induced translocation. Expression of GDP-bound (dominant negative) Rab5-S34N induces an endocytosis deficit for CB1Rs (Fig. 6*A*, *b*), shifting the MFR toward higher values for all pharmacological conditions (Fig. 6*B*, *a*). Furthermore, endocytosis of CB1Rs is reduced after incubation with WIN, suggesting that endocytosis is severely impaired. On the contrary, expression of GTP-bound (dominant active) Rab5-

Q79L favors endocytosis, leading to cells containing large aberrant vesicles (Fig. 6*A*, *c*), as described previously (13, 36). The CB1R is endocytosed into these vesicles, leading to a drop of the MFR. Interestingly, incubation with AM281 is able to externalize CB1R, but a considerable amount of receptor remains sequestered in these large vesicles (Fig. 6*B*, *a*).

Effects of Rab4 mutants (Fig. 6*A*, *d–f*) are opposite to those of Rab5 mutants, showing that Rab4 is involved in CB1R recycling. Expression of GDP-bound Rab4-S22N impairs recycling, leading to a steady-state distribution with more endocytosed receptors, and AM281 externalizes these receptors less efficiently (Fig. 6*B*, *b*). Notably, the intracellular pool of CB1Rs does not colocalize with the Rab4-S22N-EGFP (Fig. 6*A*, *e*). Furthermore, cotransfection of the GTP-bound Rab4-Q67L externalizes the receptors and is able to antagonize WIN-induced endocytosis. The remaining intracellular pool of receptors colocalizes with Rab4-Q67L-EGFP-positive vesicles (Fig. 6*A*, *f*).

Finally, constitutive endocytosis and recycling of CB1R is not dependent on Rab11, since no change occurs in the distribution and translocation of CB1R when Rab11 mutants are co-expressed (Fig. 6, *C* and *D*). CB1R does not significantly colocalize with Rab11 and seems to be largely excluded from Rab11-positive perinuclear recycling endosomes (Fig. 6*C*, *a–c*), and the few endosomes that are Rab11 and CB1R-positive are rather likely to be Rab5-, Rab11-positive sorting endosomes (37). The capacity to modify GPCR trafficking (32) of the Rab11 mutants employed in our study was verified using TfR immunolabeling. Contrary to CB1Rs, TfRs are largely present in Rab11-positive perinuclear recycling endosomes (Fig. 6*C*, *d–f*). Rab11 mutants were able to modulate TfR cycling, with enhanced plasma membrane localization of TfR in Rab11-WT- or Rab11-Q70L (GTP-bound)-transfected cells compared with nontransfected cells, whereas transfection of Rab11-S26N (GDP-bound) leads to intracellular accumulation of TfRs compared with Rab11-WT-transfected cells (data not shown). Thus, the lack of effects of Rab11 mutants on CB1R trafficking was not due to inefficient Rab11 mutants but rather to the absence of CB1R in Rab11-mediated trafficking pathways. CB1R are thus likely to constitutively cycle between plasma membrane and endosomes through Rab5-dependent constitutive endocytosis and Rab4-dependent constitutive recycling.

DISCUSSION

We have investigated spontaneous and ligand-induced intracellular translocation of CB1R in order to elucidate how an important pharmacological property of this receptor, the high level of constitutive activity (3), influences its functional trafficking. In HEK-293 cells as well as in LLC-PK1 epithelial cells or SHSY-5Y neuroblastoma cells, CB1-EGFP is predominantly localized in endosomes at steady state. Detailed analysis in HEK-293 cells shows that this distribution is a result of constitutive activity-dependent cycling of CB1R between the plasma membrane and endosomes, mediated by the small GTPases Rab5 and Rab4.

We used a GFP chimera protein to allow direct visualization of CB1R. Such fusion proteins are now widely used to study protein trafficking (38), and their usefulness is amply demonstrated for GPCRs (39, 40). In our study, we first verified that CB1-EGFP was functional by measuring constitutive inhibition of cAMP accumulation after forskolin stimulation, showing that tagged CB1-EGFP and untagged CB1-WT behaved similarly. Moreover, WIN-induced endocytosis and AM281-induced externalization were also verified after immunolabeling of CB1-WT (see Rabs-EGFP experiments), showing no differences with CB1-EGFP. Thus, CB1-EGFP is a fusion protein whose pharmacology and trafficking are similar to CB1-WT.

At steady state, CB1-EGFP is expressed on the plasma membrane, but a substantial proportion (~85% of total fluorescence) of receptors is also present in intracellular vesicles. The presence of intracellular CB1 receptors was also observed in the pioneering studies of Hsieh *et al*. (18) in AtT20 cells and of Coutts *et al*. (19) in hippocampal neurons. Intuitively, CB1R-containing intracellular vesicles could correspond to maturing receptors in the neosynthetic pathway. In fact, several constitutively active GPCRs, like mutants of the vasopressin V2 receptor (41) or the wild type δ-opioid receptor (42), are retained in the ER before reaching the cell surface, leading to a mostly intracellular phenotype. However, we found no effect of protein synthesis inhibition by cycloheximide (up to 4 h) on the intracellular distribution of CB1-EGFP. Moreover, the colocalization of CB1R-containing endosomes with Rab5- and Rab4-positive endosomes argues for localization of intracellular CB1Rs in endocytosis and recycling pathways. Finally, CB1-EGFP-positive vesicles do not significantly colocalize with organelles associated with synthesis (Golgi or ER) but rather resemble endocytic vesicles (endosomes) like those positive for TfR. The fact that only few endosomes contain both TfR and CB1R suggests that sorting events separate endocytosed CB1R and TfR, as described for the β_2-adrenergic receptor and the TfR (43). Interestingly, we also detect clear segregation between CB1R and TfR in a downstream portion of the endocytic pathway, where CB1Rs avoid Rab11-positive perinuclear recycling endosomes, whereas TfRs are enriched in this compartment.

Our data suggest that CB1Rs are constitutively endocytosed. First, antibodies that bind an extracellular epitope of CB1R in live cells are spontaneously endocytosed and subsequently found inside endosomes. Second, inhibition of clathrin-mediated endocytosis by acute depletion of plasma membrane cholesterol (27) translocates both intracellular TfRs and CB1Rs to the plasma membrane, demonstrating that endocytosis is required to generate the intracellular population of CB1Rs, similarly to TfRs. Third, spontaneous endosomal accumulation of CB1R is blocked by coexpression of a GDP-bound (inactive) mutant of Rab5 and enhanced by the GTP-bound (active) mutant. These results imply that CB1Rs are constitutively endocytosed and use Rab5-mediated postendocytotic trafficking pathways, similarly to agonist-activated GPCRs like the AT_{1A} angiotensin II receptor, the β_2 adrenergic receptor, endothelin receptors, and D2 dopamine receptors (35).

Constitutive (*i.e.* tonic) endocytosis in the absence of ligand has also been observed for other wild type GPCRs such as chemokine CXCR4 receptor (44), thyrotropin receptor (25), M2 muscarinic receptor (45), thrombin receptor (46), and thromboxane A2 receptor (47). However, these studies do not address the relationship between constitutive activity and tonic endocytosis.

The relationship between constitutive activity and constitutive endocytosis of the CB1R is revealed by the translocation effect of inverse agonist treatment. Treatment with the inverse agonist AM281 translocates intracellular CB1Rs to the plasma membrane, as first observed by Rinaldi-Carmona *et al.* (21), probably due to stabilization of the inactive form of the receptor that does not internalize. Inverse agonist-induced externalization of a constitutively active GPCRs has also been shown previously for mutants of AT_{1A} (11), for vasopressin V2, and for α_{1B} adrenergic receptor (48). The externalization process is clearly different from the up-regulation phenomenon, a general up-regulation of receptor expression level occurring after long term (~24-h) treatment with inverse agonists and requiring protein synthesis, as shown for constitutively active mutants of the α_{1B} adrenergic receptor (49). Here, the relatively short time (~2 h) necessary to reach maximal inverse agonist effect, and

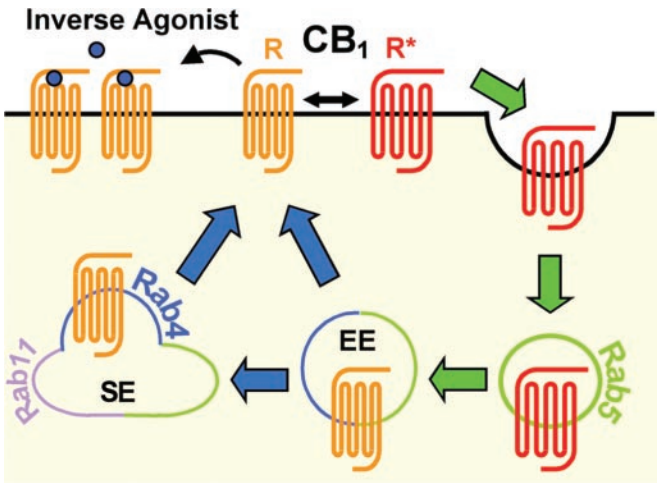

FIG. 7. **Proposed model for the constitutive trafficking of the CB1R.** Plasma membrane-localized CB1Rs are in an equilibrium between active R* (*red*) and inactive R (*orange*) states. Once activated, either constitutively or by an agonist ligand, the receptor is internalized through a Rab5-mediated pathway (*green arrow*). The receptor then travels through early endosomes (*EE*) and sorting endosomes (*SE*) and is recycled back to the plasma membrane by Rab4-mediated recycling pathways (*blue arrows*). Since recycling is slower than endocytosis, the majority of receptors are localized to endosomes at steady state. The inverse agonist, which stabilizes the inactive conformation of the receptor, leads to externalization by sequestering recycled receptors on the plasma membrane.

the constant use of cycloheximide allows to rule out protein synthesis as the primary source of externalized receptors. Furthermore, the total amount of CB1-EGFP fluorescence in cells does not change notably along the time courses studied. The alternative hypothesis of immature receptors being translocated from the ER to the plasma membrane by a chaperone effect of membrane-permeant inverse agonists, as shown for mutant vasopressin V2 receptors (41) or δ opioid receptors (50), seems also not applicable here; intracellular CB1Rs are not localized in the ER and are of endocytic origin. Furthermore, AM281-induced externalization depends on Rab4 and is blocked by monensin, showing involvement of recycling pathways.

The intracellular CB1R population could result from internalization provoked by the presence of endogenous cannabinoid ligands secreted by the cells or present in the serum-containing medium, and, in this case, AM281 would act also as an antagonist. This possibility is difficult to formally exclude, since there is no neutral antagonist for the CB1R. However, we found no significant change in the CB1R distribution when we monitored CB1-EGFP-expressing HEK-293 cells up to 3 h after incubation with fresh, ligand-free buffer (see the *control curve* in Fig. 4*C*, *b*), indicating that basal endocytosis was not due to secreted cannabinoid ligands but rather due to the constitutive activity of CB1R.

To achieve externalization, there must be a mechanism that brings CB1Rs to the plasma membrane. Here we suggest that this mechanism is a constitutive recycling process; the majority of CB1Rs externalized by the inverse agonist are probably receptors that have been previously endocytosed. This constitutive recycling is dependent on Rab4, since a GDP-bound (inactive) mutant of Rab4 promotes intracellular CB1R accumulation, whereas a GTP-bound (active) mutant leads to externalization. Rab4 is considered to drive both recycling from early endosomes and recycling endosomes (37). Rab11 has been shown to drive slow recycling from perinuclear recycling endosomes (32). CB1R does not seem to pass through Rab11-positive perinuclear recycling endosomes, and Rab11 does not intervene in constitutive trafficking of CB1R. For CB1R, the main recycling route seems to be Rab4-dependent, displaying relatively slow kinetics, since AM281-induced externalization is maximal after 2 h. Since recycling is slower than endocytosis, as shown by different kinetics of WIN and AM281 effects, the majority of CB1Rs is found in endosomes at steady state.

Thus, the CB1R is constitutively and permanently activated, endocytosed, and recycled, and inverse agonists externalize CB1R by inhibiting constitutive activation. Recently, constitutively active mutants of the AT_1 angiotensin II receptor were shown to participate in a similar cycle (11). Very recent work of Marion *et al.* (10) also reports constitutive endocytosis and inverse agonist-induced externalization of constitutively active forms of the $5HT_{2C}$ serotonin receptor, showing constitutive recruitment of β-arrestin 2. Here we extend the model of constitutive endocytosis for another constitutively active wild type GPCR, the CB1R, and we also identify the intracellular pathways implicated in this constitutive endocytosis and recycling. Our model of the constitutive trafficking cycle of CB1Rs between plasma membrane and endosomes is depicted in Fig. 7. The question of the physiological relevance of such a cycle remains open, and constitutive trafficking of CB1R in neurons is currently under investigation in our laboratory. Nevertheless, *in vivo* description of constitutively active endogenous H3 receptors (51), together with discovery of the first endogenous inverse agonists, the agouti-related peptide on the melanocortin MC1 receptor (52, 53), has paved the way toward new paradigms of GPCR physiology and deeper understanding of brain function.

Acknowledgments—We are grateful to Robert Lodge for offering the Rab-EGFP plasmids. We thank Ken Mackie for the L14 antibody and for critical reading of the manuscript. We thank Manuel Thery at the Institut Curie for four-dimensional deconvolution imaging, Sabine Bardin for help with cell culture and cellular assays, and Eric Clauser for discussion and assistance. We also thank Stéphanie Miserey-Lenkei and László Hunyady for helpful discussions and critical reading of the manuscript.

REFERENCES

1. Howard, A. D., McAllister, G., Feighner, S. D., Liu, Q., Nargund, R. P., Van der Ploeg, L. H., and Patchett, A. A. (2001) *Trends Pharmacol. Sci.* **22,** 132–140
2. Ferguson, S. S. (2001) *Pharmacol. Rev.* **53,** 1–24
3. Seifert, R., and Wenzel-Seifert, K. (2002) *Naunyn-Schmiedeberg's Arch. Pharmacol.* **366,** 381–416
4. Milligan, G., and Bond, R. A. (1997) *Trends Pharmacol. Sci.* **18,** 468–474
5. Matsuda, L. A., Lolait, S. J., Brownstein, M. J., Young, A. C., and Bonner, T. I. (1990) *Nature* **346,** 561–564
6. Howlett, A. C., Barth, F., Bonner, T. I., Cabral, G., Casellas, P., Devane, W. A., Felder, C. C., Herkenham, M., Mackie, K., Martin, B. R., Mechoulam, R., and Pertwee, R. G. (2002) *Pharmacol. Rev.* **54,** 161–202
7. Bouaboula, M., Perrachon, S., Milligan, L., Canat, X., Rinaldi-Carmona, M., Portier, M., Barth, F., Calandra, B., Pecceu, F., Lupker, J., Maffrand, J. P., Le Fur, G., and Casellas, P. (1997) *J. Biol. Chem.* **272,** 22330–22339
8. Pan, X., Ikeda, S. R., and Lewis, D. L. (1998) *Mol. Pharmacol.* **54,** 1064–1072
9. Hillard, C. J., Muthian, S., and Kearn, C. S. (1999) *FEBS Lett.* **459,** 277–281
10. Marion, S., Weiner, D. M., and Caron, M. G. (2004) *J. Biol. Chem.* **279,** 2945–2954
11. Miserey-Lenkei, S., Parnot, C., Bardin, S., Corvol, P., and Clauser, E. (2002) *J. Biol. Chem.* **277,** 5891–5901
12. Kobayashi, T., Stang, E., Fang, K. S., de Moerloose, P., Parton, R. G., and Gruenberg, J. (1998) *Nature* **392,** 193–197
13. Hunyady, L., Baukal, A. J., Gaborik, Z., Olivares-Reyes, J. A., Bor, M., Szaszak, M., Lodge, R., Catt, K. J., and Balla, T. (2002) *J. Cell Biol.* **157,** 1211–1222
14. Darmon, M., Langlois, X., Suffisseau, L., Fattaccini, C. M., and Hamon, M. (1998) *J. Neurochem.* **71,** 2294–2303
15. Savino, T. M., Gebrane-Younes, J., De Mey, J., Sibarita, J. B., and Hernandez-Verdun, D. (2001) *J. Cell Biol.* **153,** 1097–1110
16. Lenkei, Z., Beaudet, A., Chartrel, N., De Mota, N., Irinopoulou, T., Braun, B., Vaudry, H., and Llorens-Cortes, C. (2000) *J. Histochem. Cytochem.* **48,** 1553–1564
17. Landsman, R. S., Burkey, T. H., Consroe, P., Roeske, W. R., and Yamamura, H. I. (1997) *Eur. J. Pharmacol.* **334,** R1–R2
18. Hsieh, C., Brown, S., Derleth, C., and Mackie, K. (1999) *J. Neurochem.* **73,** 493–501
19. Coutts, A. A., Anavi-Goffer, S., Ross, R. A., MacEwan, D. J., Mackie, K., Pertwee, R. G., and Irving, A. J. (2001) *J. Neurosci.* **21,** 2425–2433
20. Roche, J. P., Bounds, S., Brown, S., and Mackie, K. (1999) *Mol. Pharmacol.* **56,** 611–618

21. Rinaldi-Carmona, M., Le Duigou, A., Oustric, D., Barth, F., Bouaboula, M., Carayon, P., Casellas, P., and Le Fur, G. (1998) *J. Pharmacol. Exp. Ther.* **287,** 1038–1047
22. Jin, W., Brown, S., Roche, J. P., Hsieh, C., Celver, J. P., Kovoor, A., Chavkin, C., and Mackie, K. (1999) *J. Neurosci.* **19,** 3773–3780
23. Gatley, S. J., Lan, R., Pyatt, B., Gifford, A. N., Volkow, N. D., and Makriyannis, A. (1997) *Life Sci.* **61,** 191–197
24. Hillard, C. J., Manna, S., Greenberg, M. J., DiCamelli, R., Ross, R. A., Stevenson, L. A., Murphy, V., Pertwee, R. G., and Campbell, W. B. (1999) *J. Pharmacol. Exp. Ther.* **289,** 1427–1433
25. Baratti-Elbaz, C., Ghinea, N., Lahuna, O., Loosfelt, H., Pichon, C., and Milgrom, E. (1999) *Mol. Endocrinol.* **13,** 1751–1765
26. Tsao, P., Cao, T., and von Zastrow, M. (2001) *Trends Pharmacol. Sci.* **22,** 91–96
27. Subtil, A., Gaidarov, I., Kobylarz, K., Lampson, M. A., Keen, J. H., and McGraw, T. E. (1999) *Proc. Natl. Acad. Sci. U. S. A.* **96,** 6775–6780
28. van Dam, E. M., and Stoorvogel, W. (2002) *Mol. Biol. Cell* **13,** 169–182
29. van Dam, E. M., Ten Broeke, T., Jansen, K., Spijkers, P., and Stoorvogel, W. (2002) *J. Biol. Chem.* **277,** 48876–48883
30. Zerial, M., and McBride, H. (2001) *Nat. Rev. Mol. Cell. Biol.* **2,** 107–117
31. Bucci, C., Parton, R. G., Mather, I. H., Stunnenberg, H., Simons, K., Hoflack, B., and Zerial, M. (1992) *Cell* **70,** 715–728
32. Ullrich, O., Reinsch, S., Urbe, S., Zerial, M., and Parton, R. G. (1996) *J. Cell Biol.* **135,** 913–924
33. van der Sluijs, P., Hull, M., Webster, P., Male, P., Goud, B., and Mellman, I. (1992) *Cell* **70,** 729–740
34. Rosenfeld, J. L., Knoll, B. J., and Moore, R. H. (2002) *Receptors Channels* **8,** 87–97
35. Seachrist, J. L., and Ferguson, S. S. (2003) *Life Sci.* **74,** 225–235
36. Seachrist, J. L., Laporte, S. A., Dale, L. B., Babwah, A. V., Caron, M. G., Anborgh, P. H., and Ferguson, S. S. (2002) *J. Biol. Chem.* **277,** 679–685
37. Sonnichsen, B., De Renzis, S., Nielsen, E., Rietdorf, J., and Zerial, M. (2000) *J. Cell Biol.* **149,** 901–914
38. Lippincott-Schwartz, J., and Smith, C. L. (1997) *Curr. Opin. Neurobiol.* **7,** 631–639
39. Daly, C. J., and McGrath, J. C. (2003) *Pharmacol. Ther.* **100,** 101–118
40. Kallal, L., and Benovic, J. L. (2000) *Trends Pharmacol. Sci.* **21,** 175–180
41. Morello, J. P., Salahpour, A., Laperriere, A., Bernier, V., Arthus, M. F., Lonergan, M., Petaja-Repo, U., Angers, S., Morin, D., Bichet, D. G., and Bouvier, M. (2000) *J. Clin. Invest.* **105,** 887–895
42. Petaja-Repo, U. E., Hogue, M., Laperriere, A., Walker, P., and Bouvier, M. (2000) *J. Biol. Chem.* **275,** 13727–13736
43. Cao, T. T., Mays, R. W., and von Zastrow, M. (1998) *J. Biol. Chem.* **273,** 24592–24602
44. Signoret, N., Oldridge, J., Pelchen-Matthews, A., Klasse, P. J., Tran, T., Brass, L. F., Rosenkilde, M. M., Schwartz, T. W., Holmes, W., Dallas, W., Luther, M. A., Wells, T. N., Hoxie, J. A., and Marsh, M. (1997) *J. Cell Biol.* **139,** 651–664
45. Roseberry, A. G., and Hosey, M. M. (1999) *J. Biol. Chem.* **274,** 33671–33676
46. Shapiro, M. J., Trejo, J., Zeng, D., and Coughlin, S. R. (1996) *J. Biol. Chem.* **271,** 32874–32880
47. Fraile-Ramos, A., Kledal, T. N., Pelchen-Matthews, A., Bowers, K., Schwartz, T. W., and Marsh, M. (2001) *Mol. Biol. Cell* **12,** 1737–1749
48. Wilbanks, A. M., Laporte, S. A., Bohn, L. M., Barak, L. S., and Caron, M. G. (2002) *Biochemistry* **41,** 11981–11989
49. Stevens, P. A., Bevan, N., Rees, S., and Milligan, G. (2000) *Mol. Pharmacol.* **58,** 438–448
50. Petaja-Repo, U. E., Hogue, M., Bhalla, S., Laperriere, A., Morello, J. P., and Bouvier, M. (2002) *EMBO J.* **21,** 1628–1637
51. Morisset, S., Rouleau, A., Ligneau, X., Gbahou, F., Tardivel-Lacombe, J., Stark, H., Schunack, W., Ganellin, C. R., Schwartz, J. C., and Arrang, J. M. (2000) *Nature* **408,** 860–864
52. Nijenhuis, W. A., Oosterom, J., and Adan, R. A. (2001) *Mol. Endocrinol.* **15,** 164–171
53. Haskell-Luevano, C., and Monck, E. K. (2001) *Regul. Pept.* **99,** 1–7